JOURNAL OF CATALYSIS **158,** 170–180 (1996)
ARTICLE NO. 0016

A Microkinetic Analysis of the Water–Gas Shift Reaction under Industrial Conditions

C. V. Ovesen,* B. S. Clausen,* B. S. Hammershøi,* G. Steffensen,* T. Askgaard,† I. Chorkendorff,† J. K. Nørskov,†‡ P. B. Rasmussen,† P. Stoltze,†‡ and P. Taylor†

*Haldor Topsøe Research Laboratories, DK-2800 Lyngby, Denmark; †Physics Department, Technical University of Denmark, DK-2800 Lyngby, Denmark; and ‡Center for Atomic-scale Materials Physics, Technical University of Denmark, DK-2800 Lyngby, Denmark

Received August 24, 1994; revised May 9, 1995; accepted August 21, 1995

To form the basis for a microkinetic understanding of the low-temperature water–gas shift reaction over Cu-based catalysts as operated industrially, the kinetics have been measured under a wide range of reaction conditions. To elucidate possible support effects the reaction was studied over catalysts of Cu supported on Al_2O_3, SiO_2, or mixed ZnO/Al_2O_3. The proposed microkinetic model is based on a "surface redox" mechanism deduced from Cu single-crystal studies. All the input data for the elementary steps were taken from available Cu single-crystal studies and the total number of sites was the only free parameter in the microkinetic analysis. It was found to be important especially at high pressure to include in the mechanism the synthesis and hydrogenation of formate. The different dependencies of the overall kinetics have also been evaluated by a power law kinetic model, which was found to give an excellent representation of the kinetic data. It is seen that in spite of the severe constraints placed on the microkinetic model it could account for many of the important kinetic dependencies of the industrial water–gas shift reaction over the different Cu-based catalysts. Furthermore, the deduced number of active sites agrees well with the initial Cu surface area of the reduced catalysts determined separately by H_2-TPD suggesting that the model is also satisfactory for describing quantitatively the magnitude of the rates. Thus, a good starting point in interpreting the water–gas shift kinetics is to consider the catalysis occurring solely on the metallic Cu particles in the catalysts. The nature of the support may, however, have important secondary roles. For example, dynamic restructuring of the Cu particles may take place by changing the synthesis conditions and may depend on the nature of the support, as recently evidenced in separate EXAFS experiments.

1. INTRODUCTION

The water–gas shift reaction

$$CO + H_2O \rightleftharpoons CO_2 + H_2 \qquad [1]$$

is industrially a very important reaction (1–4). It is used to increase the H_2 content in synthesis gas and is an important part of an ammonia or a hydrogen plant. The industrial low-temperature water–gas shift catalyst consists of a combination of Cu, ZnO, and Al_2O_3. The reaction is typically performed at 473 K, 30 atm, and a steam to dry gas ratio of 0.4 with a dry gas composition of 2% CO, 20% CO_2, and 78% H_2.

The kinetics of the water–gas shift reaction over Cu-based catalysts have been studied by several groups (5–10). However, these previous studies were all at low pressure and with a gas composition far from that used industrially. In the present work we have studied the kinetics of the water–gas shift reaction under industrial conditions. In addition, the reaction has been studied over three different Cu-based catalysts, $Cu/ZnO/Al_2O_3$, Cu/Al_2O_3, and Cu/SiO_2.

It is well known that an accurate description of the measured reaction rates from a data set can be obtained from an expression where all kinetic parameters are fitted, for example, to a power law. Such empirical kinetic expressions are essential in reactor design calculations where it is necessary to have a very accurate description of the reaction rate. However, it is also well known that different mechanisms can lead to the same overall kinetic expression, see, e.g., Refs. (11, 12). For this reason it is difficult to determine the mechanism from an empirical kinetic expression.

In view of this there is an interest in developing microkinetic models based on the knowledge about elementary steps and their energetics (11, 13). From a microkinetic model it is possible to estimate surface coverages, reaction orders, and activation enthalpy during reaction conditions. For this reason, the applicability of the microkinetic model is not restricted to a particular set of conditions but can be used under various conditions where simplified models may break down. This is, for example, very important in processes where very large concentration changes are encountered, as in environmental catalysis (14, 15). Thus the advantage of a microkinetic model is to explore the

0021-9517/96 $12.00

chemistry of a given reaction whereas the advantage of an empirical kinetic model is that it provides a very accurate description of the reaction rate, which is essential in reactor design calculations.

We have chosen to analyze the present kinetic data using as a starting point the microkinetic model developed by Ovesen *et al.* (16). One of the aims has been to test to what extent one can explain the magnitude of the rate and the kinetic trends by constraining the model input parameters to those obtained from Cu single-crystal surface science studies.

2. EXPERIMENTAL

Continuous-flow equipment with a tubular reactor was used to obtain the kinetic data. The feed gases were fed from premixed gas bottles and the flows were controlled by electronic mass flow meters. Sulfur and chlorine impurities in the gases were removed by means of a zinc oxide and a copper zinc oxide catalyst (Haldor Topsøe's LSK and LK-821 catalysts) operating at ambient temperature. Ion-exchanged and degassed water was fed by a high-precision pump and evaporated in a heated stainless-steel tube leading to the reactor inlet. The tubular stainless-steel plug flow reactor which was Cu lined was externally heated and the temperature was measured by use of a chromel-alumel thermocouple placed in the center of the catalyst bed. The reactor was charged with 0.1 to 0.2 g of catalyst with particle sizes between 0.5 and 0.8 mm mixed with crushed alumina to assure a minimum bed height of 75 mm. A gas chromatograph with a system of packed and capillary columns was used to analyze the product gases after condensation and removal of the water.

Three types of Cu-based catalyst were used in the experiments, $Cu/ZnO/Al_2O_3$, Cu/Al_2O_3, and Cu/SiO_2. The $Cu/ZnO/Al_2O_3$ catalyst contained about 40% Cu, 22% Zn, and 5% Al. The binary Cu/Al_2O_3 catalyst was prepared according to the procedure given in Ref. (17) and contained 35% Cu, whereas the binary Cu/SiO_2 catalyst containing 21% Cu was prepared according to the procedure given in Ref. (18). Activation was performed at atmospheric pressure by heating the catalysts in a gas mixture containing 0.5% CO, 4% CO_2, and 4% H_2 in He with a ramp of 0.6 K/min to 493 K. The kinetic measurements were carried out for the $Cu/ZnO/Al_2O_3$ catalyst at both 5 bar and about 20 bar and for the Cu/Al_2O_3 and Cu/SiO_2 catalysts at 20 bar. The temperature was varied over a range of temperatures (453 to 493 K). For the $Cu/ZnO/Al_2O_3$ and Cu/Al_2O_3 catalysts the following dry gas compositions were used:

1. 2.5% CO, 22% CO_2, balance H_2
2. 2.5% CO, 11% CO_2, 73% H_2, balance He
3. 2.5% CO, 22% CO_2, 40% H_2, balance He.

The Cu/SiO_2 catalyst was exposed to gas 1 and in addition to gas 4:

4. 25% CO_2, balance H_2

in order to study the kinetics of the reverse water–gas shift reaction. The steam to dry gas ratio was varied between 0.2 and 0.7 for all catalysts.

The catalyst was allowed to stabilize for a few days under synthesis conditions to avoid extensive corrections for loss in catalyst activity during the subsequent kinetic measurements. To follow possible catalyst deactivation, data under a given set of conditions were frequently measured. Experiments were performed to ensure that the data were not affected by mass transport or back mixing.

The copper surface area of the catalysts after reduction was measured independently by an H_2-TPD technique (19) and the values for the three catalysts were

$Cu/ZnO/Al_2O_3$,	10 m^2/g
Cu/Al_2O_3,	15 m^2/g
Cu/SiO_2,	5 m^2/g.

Most of the kinetic measurements were made at approximately constant space velocity with varying temperature and gas composition. However, this type of kinetic measurement can give correlation between the variation in one parameter and the conversion. This is undesirable when using the measurements to determine kinetic parameters in a macroscopic kinetic model. For this reason activity measurements in which a constant conversion was achieved by varying the space velocity were also carried out. A selection of the experimental data is given in the appendix.

3. ANALYSIS OF KINETIC DATA

3.1. Microkinetic Model

Previously Ovesen *et al.* (16) have developed a microkinetic model of the low-temperature water–gas shift reaction. The model is based on the "surface redox" mechanism deduced from available single-crystal studies of the reaction of CO, CO_2, H_2, and H_2O on Cu surfaces (10, 16):

1. $H_2O(g) + * \rightleftharpoons H_2O*$
2. $H_2O* + * \rightleftharpoons OH* + H*$
3. $2OH* \rightleftharpoons H_2O* + O*$
4. $OH* + * \rightleftharpoons O* + H*$
5. $2H* \rightleftharpoons H_2(g) + 2*$
6. $CO(g) + * \rightleftharpoons CO*$
7. $CO* + O* \rightleftharpoons CO_2* + *$
8. $CO_2* \rightleftharpoons CO_2(g) + *$,

where the asterisk signifies a free surface site and $X*$ is an adsorbed species. The name surface redox mechanism refers to the situation where H_2O is dissociated completely on the surface to $O*$ and H_2 and the $O*$ is then titrated

TABLE 1

Rate and Equilibrium Equations for Kinetic Model Based on Reaction Steps 1 to 8 (k_i Is Forward Rate Constant, K_i Equilibrium Constant, and θ_i Surface Coverage of Species i)

$$K_1 \frac{P_{H_2O}}{P_0} = \theta_{H_2O^*}$$

$$r_2 = k_2\theta_{H_2O^*}\theta_* - \frac{k_2}{K_2}\theta_{OH^*}\theta_{H^*}$$

$$K_3\theta_{OH^*}^2 = \theta_{H_2O^*}\theta_{O^*}$$

$$r_4 = k_4\theta_{OH^*}\theta_* - \frac{k_4}{K_4}\theta_{O^*}\theta_{H^*}$$

$$K_5\theta_{H^*}^2 = \frac{P_{H_2}}{P_0}\theta_*^2$$

$$K_6\frac{P_{CO}}{P_0}\theta_* = \theta_{CO^*}$$

$$r_7 = k_7\theta_{CO^*}\theta_{O^*} - \frac{k_7}{K_7}\theta_{CO_2^*}\theta_*$$

$$K_8\theta_{CO_2^*} = \frac{P_{CO_2}}{P_0}\theta_*$$

by CO. The model describes the kinetics of adsorption and desorption of CO, CO_2, H_2, and H_2O, the kinetics of dissociation of H_2O and of oxidation of CO, and the kinetics and thermodynamics of the overall reaction (16).

The expressions for the rate and equilibrium equations that constitute the model are shown in Table 1. It is seen that under given reaction conditions the model describes the coverage of surface species in addition to the overall rate. From the model it is also possible to derive an analytical expression for the overall activation enthalpy $H^{\neq}$ of the reaction (16) as $H^{\neq}$ is defined by

$$H^{\neq} = k_B T^2 \left(\frac{d\ln r_+}{dT}\right)_p, \qquad [2]$$

where k_B is Boltzmann's constant and r_+ is the forward rate of the reaction. Similarly it is possible to derive an analytical expression for the reaction order α_i of component i (16) as α_i is defined by

$$\alpha_i = \left(\frac{d\ln r_+}{d\ln(p_i/p_0)}\right). \qquad [3]$$

The expressions for $H^{\neq}$ and α_i, where reaction step 7, the oxidation of CO, is assumed rate limiting and dissociation of water is in equilibrium, are shown in Table 2. It is seen that there is a simple relation between $H^{\neq}$ and the coverage of surface species. $H^{\neq}$ is a sum of the activation enthalpy for the rate-limiting step and a weighted average of the desorption enthalpies for the intermediates. The average is formed by multiplying the coverage of the intermediates by twice the enthalpy of desorption for the intermediates through equilibrium steps. The factor of two enters as the rate-limiting step requires two free sites. $H^{\neq}$ is thus the sum of the activation enthalpy of the rate-limiting step plus the average cost of creating two free sites on the surface. Similarly the reaction orders are found to be related to the coverage of surface species.

When the model was tested against measurements for an industrial ($Cu/ZnO/Fe_2O_3$) catalyst at 1 atm performed by van Herwijnen and de Jong (5), a good agreement was found (16, 20). It was concluded that the catalyst appears to expose Cu(111) facets almost exclusively. It was also found that reaction step 2 is rate limiting in a gas with a low ratio of water to carbon monoxide whereas reaction step 7 is rate limiting in a gas with a high ratio of water to carbon monoxide. Reaction 4 is extremely slow and only gives a significant contribution for reactions in a CO_2 + H_2 mixture. The synthesis of formate was excluded in the above mechanism. From the kinetics of synthesis and decomposition of formate observed on Cu(100) exposed to H_2 + CO_2 (21) the stability of formate was estimated and it was concluded that formate was not present in significant amounts at 1 atm. Although carbonate has been suggested as an intermediate in both methanol synthesis and the water–gas shift reaction [see, for instance, Ref. (22)], the synthesis of carbonate was excluded from the mechanism since attempts to synthesize carbonate by exposing a Cu single-crystal surface precovered with oxygen to CO_2 all

TABLE 2

Overall Activation Enthalpy $H^{\neq}$ and Reaction Orders α_i when Reaction Step 7 (Oxidation of CO) Is Assumed Rate Limiting

$$H^{\neq} = H_7^{\neq} + H_1 + 2H_2 + H_3 + H_5 + H_6 - 2H_1\theta_{H_2O^*} - 2H_6\theta_{CO^*} + 2H_8\theta_{CO_2^*} - 2(H_1 + 2H_2 + H_3 + H_5)\theta_{O^*} + H_5\theta_{H^*} - 2\left(H_1 + H_2 + \frac{1}{2}H_5\right)\theta_{OH^*}$$

$$\alpha_{H_2O} = 1 - 2(\theta_{H_2O^*} + \theta_{OH^*} + \theta_{O^*})$$

$$\alpha_{CO} = 1 - 2\theta_{CO^*}$$

$$\alpha_{CO_2} = -2\theta_{CO_2^*}$$

$$\alpha_{H_2} = -1 + \theta_{OH^*} - \theta_{H^*} + 2\theta_{O^*}$$

Note. H_1 to H_8 is the reaction enthalpy for reaction steps 1 to 8. $H_7^{\neq}$ is the activation enthalpy for reaction step 7.

TABLE 3

Rate and Equilibrium Equations for Synthesis of Formate

$$K_9\theta_{CO_2*}\theta_{H*} = \theta_{HCOO*}\theta_*$$

$$r_{10} = k_{10}\theta_{HCOO*}\theta_{H*} - \frac{k_{10}}{K_{10}}\theta_{H_2COO*}\theta_*$$

$$K_{11}\theta_{H_2COO*}\theta_{H*}^4 = P_{CH_3OH}P_{H_2O}\theta_*^5$$

Note. The equations complete the proposed kinetic model for the water–gas shift reaction under industrial conditions. k_i is forward rate constant, K_i equilibrium constant, and θ_i surface coverage of species i.

showed that carbonate was not formed under these conditions (23, 24).

When this model [Table 1, (16)] is tested against the new kinetic high-pressure data some deviation between the calculated and the experimental rate is found. Compared to the results of the macroscopic power law analysis the activation enthalpy is too low and the reaction order for CO_2 should be negative instead of zero. In the original model the reaction order for CO_2 is determined by the coverage of CO_2* (Table 2). CO_2* is weakly bound to the surface and the coverage of CO_2* is therefore low, leading to a reaction order for CO_2 of approximately zero. In order for the reaction to be more inhibited by CO_2 there must be another species present on the surface that is in equilibrium with CO_2 in the gas phase. Since CO_2 is a product of the shift reaction this will lead to a negative reaction order for CO_2. Furthermore, the presence of another species on the surface will lead to a higher apparent activation enthalpy, since the activation enthalpy is directly related to the coverage of intermediates on the surface (Table 2).

Returning to the synthesis of formate, the estimate of the stability of this species shows that the coverage of formate is significant at high pressure. Since formate is synthesized from CO_2 and H_2 (21, 25) the inclusion of the synthesis of formate in the mechanism can then lead to a higher apparent activation energy and a negative reaction order for CO_2 giving a better description of the kinetics.

From studies of the kinetics of the synthesis (21), decomposition (21), and hydrogenation (26) of formate on Cu(100) exposed to $H_2 + CO_2$ and from studies of the synthesis of methanol on Cu(100) exposed to $H_2 + CO_2$ (27) the following mechanism for formate synthesis and hydrogenation has been deduced:

9. $CO_2* + H* \rightleftharpoons HCOO* + *$
10. $HCOO* + H* \rightleftharpoons H_2COO* + *$
11. $H_2COO* + 4H* \rightleftharpoons CH_3OH(g) + H_2O(g) + 5*$.

Formate is synthesized from adsorbed hydrogen and carbon dioxide in reaction step 9. In addition to the decomposition of formate through the reverse of reaction step 9, formate can undergo hydrogenation through reaction steps 10 and 11. Reaction step 11 consists of several elementary steps. A proposal for these steps and a detailed discussion is given in Refs. (20, 27). Use of the estimated rate and equilibrium constants for reaction steps 9, 10, and 11 (21, 26) shows that reaction step 9 is in equilibrium under the industrial conditions of the water–gas shift reaction. Whether reaction step 10 or a step following reaction step 10 is assumed rate limiting is not important for the present discussion since the coverage of H_2COO* is always low.

For considering the kinetics of the water–gas shift reaction at industrial conditions it is necessary to include a description of the synthesis of formate. Thus, in addition to the rate and equilibrium equations in Table 1 the present kinetic model includes the rate and equilibrium equation for steps 9, 10, and 11, as shown in Table 3. The effect of the inclusion of these equations on the activation enthalpy and the reaction orders is shown in Table 4. It is seen that the inclusion of the synthesis of formate affects the overall activation enthalpy and the reaction order for H_2 and CO_2. The mechanism for the high-pressure water–gas shift reaction considered here then consists of the reaction sequence of steps 1 through 11 with reaction steps 2, 4, 7, and 10 as possible slow steps. In this mechanism, formate may be present on the surface, but since it is not a species in the catalytic cycle for CO conversion to CO_2 it is a ''dead end'' in the water–gas shift reaction and its effect is mainly to block the active sites.

The rate constants in the model are described by the Arrhenius equation and the equilibrium constants are calculated from the partition functions of the intermediates (16). The partition function of a specific molecule is calculated from the vibrational frequencies and the ground state energy of the molecule. The vibrational frequencies of an adsorbed molecule are taken from HREELS spectra whereas the ground state energy is determined from TPD spectra. A detailed description of the procedure is given in Ref. (16). The parameters used in the model are taken from available studies of the kinetics of the adsorption and desorption of H_2, H_2O, CO, and CO_2, the dissociation of H_2O, and the oxidation of CO over the Cu(111) plane and are published in Ref. (16). In addition parameters for synthesis and hydrogenation of formate on Cu(100) have been deduced (21, 26).

In the present study the parameters for Cu(100) are used in the treatment of reaction step 9 through 11 since these reactions have not been studied over Cu(111). This may also be a reasonable choice in the sense that Cu(100) and Cu(111) have approximately the same surface density.

The parameters used in the model are shown in Table 5. It is stressed that the present model with the parameters

TABLE 4

Overall Activation Enthalpy $H^{\neq}$ and Reaction Orders α_i when Reaction Step 7 Oxidation of CO Is Assumed Rate Limiting and Synthesis of Formate Reaction Step 9 Is Included in the Mechanism

$$H^{\neq} = H_7^{\neq} + H_1 + 2H_2 + H_3 + H_5 + H_6 - 2H_1\theta_{H_2O^*} - 2H_6\theta_{CO^*} + 2H_8\theta_{CO_2^*}$$
$$- 2(H_1 + 2H_2 + H_3 + H_5)\theta_{O^*} + H_5\theta_{H^*} - 2\left(H_1 + H_2 + \frac{1}{2}H_5\right)\theta_{OH^*}$$
$$+ 2\left(\frac{1}{2}H_5 + H_8 - H_9\right)\theta_{HCOO^*} + 2(H_5 + H_8 - H_9 - H_{10})\theta_{H_2COO^*}$$

$$\alpha_{H_2O} = 1 - 2(\theta_{H_2O^*} + \theta_{OH^*} + \theta_{O^*})$$

$$\alpha_{CO} = 1 - 2\theta_{CO^*}$$

$$\alpha_{CO_2} = -2\theta_{CO_2^*} - 2\theta_{HCOO^*} - 2\theta_{H_2COO^*}$$

$$\alpha_{H_2} = -1 + \theta_{OH^*} - \theta_{H^*} + 2\theta_{O^*} - \theta_{HCOO^*} - 2\theta_{H_2COO^*}$$

Note. H_1 to H_{10} is the reaction enthalpy for reaction step 1 to 10. $H_7^{\neq}$ is the activation enthalpy for reaction step 7.

listed in Table 5 cannot be used to calculate the rate of methanol synthesis. The reason is that a detailed analysis of the rate-limiting step has not been performed. For more detailed information of these reactions the reader is referred to Refs. (20, 27).

The kinetic equations 1 through 11 are solved for the coverages and the overall reaction rate. The integration through the plug flow reactor is done by an adaptive step-size Runge–Kutta procedure.

The activity measurements under standard conditions show that the catalyst deactivates slightly with time on stream. These measurements have been used to establish

TABLE 5

Table of Thermodynamic and Kinetic Data Used in the Microkinetic Model

H_2(g)	$\omega = 4405\ cm^{-1}$, $B = 60.8\ cm^{-1}$, $\sigma = 2$, $E_g = -35$ kJ/mol
H*	$\omega_\perp = 1291\ cm^{-1}$, $\omega_\parallel = 157\ cm^{-1}$, $E_g = -27$ kJ/mol
H_2O(g)	$\omega_1 = 1595\ cm^{-1}$, $\omega_2 = 3657\ cm^{-1}$, $\omega_3 = 3756\ cm^{-1}$, $\sigma = 2$, $I_AI_BI_C = 5.7658 \times 10^{-141}\ kg^3\ m^6$, $E_g = -306$ kJ/mol
H_2O*	$\omega_1 = 1600\ cm^{-1}$, $\omega_2 = 3370\ cm^{-1}$ $\omega_3 = 3370\ cm^{-1}$ $\omega_4 = 745\ cm^{-1}$, $\omega_\perp = 460\ cm^{-1}$, $\omega_\parallel = 21\ cm^{-1}$, $E_g = -359$ kJ/mol
O*	$\omega_\perp = 391\ cm^{-1}$, $\omega_\parallel = 508\ cm^{-1}$, $E_g = -243$ kJ/mol
OH*	$\omega = 3380\ cm^{-1}$, $\omega_\perp = 280\ cm^{-1}$, $\omega_\parallel = 670\ cm^{-1}$, $E_g = -319$ kJ/mol
CO(g)	$\omega = 2170\ cm^{-1}$, $B = 1.9\ cm^{-1}$, $\sigma = 1$, $E_g = -130$ kJ/mol
CO*	$\omega = 2077\ cm^{-1}$, $\omega_\perp = 330\ cm^{-1}$, $\omega_\parallel = 17\ cm^{-1}$, $E_g = -181$ kJ/mol
CO_2(g)	$\omega_1 = 1343\ cm^{-1}$, $\omega_2 = 667\ cm^{-1}$, $\omega_3 = 2349\ cm^{-1}$, $B = 0.39\ cm^{-1}$, $\sigma = 2$, $E_g = -431$ kJ/mol
CO_2*	$\omega_1 = 1600\ cm^{-1}$, $\omega_2 = 3370\ cm^{-1}$, $\omega_3 = 3370\ cm^{-1}$, $\omega_4 = 745\ cm^{-1}$, $\omega_\perp = 460\ cm^{-1}$, $\omega_\parallel = 21\ cm^{-1}$, $E_g = -359$ kJ/mol
HCOO*	$\omega_1 = 760\ cm^{-1}$, $\omega_2 = 1330\ cm^{-1}$, $\omega_3 = 1640\ cm^{-1}$, $\omega_4 = 2910\ cm^{-1}$, $\omega_5 = 1043\ cm^{-1}$, $\omega_6 = 1377\ cm^{-1}$, $\omega_7 = 1377\ cm^{-1}$ $\omega_\perp = 340\ cm^{-1}$, $\omega_\parallel = 36\ cm^{-1}$, $E_g = -554$ kJ/mol
H_2COO*	$\omega_1 = 630\ cm^{-1}$, $\omega_2 = 960\ cm^{-1}$, $\omega_3 = 1090\ cm^{-1}$, $\omega_4 = 1220\ cm^{-1}$, $\omega_5 = 1420\ cm^{-1}$, $\omega_6 = 1480\ cm^{-1}$, $\omega_7 = 2920\ cm^{-1}$, $\omega_8 = 3000\ cm^{-1}$, $\omega_9 = 400\ cm^{-1}$ $\omega_\perp = 405\ cm^{-1}$, $\omega_\parallel = 30\ cm^{-1}$, $E_g = -568$ kJ/mol
CH_3OH(g)	$\omega_1 = 270\ cm^{-1}$, $\omega_2 = 1033\ cm^{-1}$, $\omega_3 = 1060\ cm^{-1}$, $\omega_4 = 1165\ cm^{-1}$, $\omega_5 = 1345\ cm^{-1}$, $\omega_6 = 1477\ cm^{-1}$, $\omega_7 = 1455\ cm^{-1}$, $\omega_8 = 2844\ cm^{-1}$, $\omega_9 = 2960\ cm^{-1}$, $\omega_{10} = 3000\ cm^{-1}$, $\omega_{11} = 3681\ cm^{-1}$ $I_AI_BI_C = 7897 \times 10^{-141}\ kg^3\ m^6$, $E_g = -343$ kJ/mol
k_2	$A_2 = 9.90 \times 10^{13}\ s^{-1}$, $E_2 = 114$ kJ/mol
k_7	$A_7 = 3.4 \times 10^{12}\ s^{-1}$, $E_7 = 64$ kJ/mol
k_{10}	$A_{10} = 3.2 \times 10^{9}\ s^{-1}$, $E_{10} = 79$ kJ/mol

Note. ω vibrational frequency, B rotational constant, σ symmetry number, E_g ground state energy, and $I_AI_BI_C$ product of moments of inertia.

a relation between catalyst activity and time on stream using the deactivation model described in (28).

3.2. Power Law Model

As a macroscopic kinetic model we have used the following power law expression (29)

$$r = A \cdot \exp(-E_a/\mathrm{RT}) \cdot P_{\mathrm{CO}}^{\alpha\mathrm{CO}} \cdot P_{\mathrm{H_2O}}^{\alpha\mathrm{H_2O}} \cdot P_{\mathrm{CO_2}}^{\alpha\mathrm{CO_2}} \cdot P_{\mathrm{H_2}}^{\alpha\mathrm{H_2}} \cdot P_{\mathrm{tot}}^{\gamma} \cdot (1-\beta), \quad [4]$$

where

$$\beta = \frac{1}{K_g} \cdot \frac{(P_{\mathrm{CO_2}} \cdot P_{\mathrm{H_2}})}{(P_{\mathrm{CO}} \cdot P_{\mathrm{H_2O}})}.$$

A is the preexponential factor, E_a is the apparent activation enthalpy, P_i the partial pressure of component i, α_i is the apparent reaction order of component i, P_{tot} is the total pressure, γ is a fudge factor correcting the total pressure dependence, β is the approach to equilibrium, and K_g is the equilibrium constant for the water–gas shift reaction.

For reaction data at the same total pressure γ has been set to zero and A, E_a, α_i have been estimated to obtain the minimum sum of squares between the model and the experimental data. As mentioned above, the activity measurements under standard conditions show that the catalyst deactivates slightly with time on stream. The estimates of parameters take into account a correction of this deactivation.

For the experiments over Cu/SiO_2 only the steam to dry gas ratio was varied. There is therefore not sufficient information in the data set to make a reliable parameter estimate using Eq. [4] and the kinetic data for Cu/SiO_2 have not been analyzed with the power law model.

An analysis of the kinetic data sets for Cu/Al_2O_3 and for $Cu/ZnO/Al_2O_3$ show that there are correlations between variation in the partial pressures and temperature in the kinetic measurements. It is possible to obtain a good fit to the reaction data sets with Eq. [4] but with somewhat different solutions. Therefore it was decided to use the measurements where essentially only the concentration of CO is varied (measurements for constant gas composition but varying space velocity) to estimate the apparent reaction order for CO separately. An analysis of these data shows that an apparent reaction order for CO of unity gives the best representation of the data. α_{CO} has therefore been fixed to unity in the parameter estimation. The results of the parameter estimate are shown in Table 6. We find that the apparent activation enthalpy and reaction orders determined at 5 and 20 bar for the reaction data for the $Cu/ZnO/Al_2O_3$ catalyst are very similar. Despite this, it was necessary to introduce the fudge factor γ correcting the total pressure dependency to make the power law model estimated at 5 bar applicable at 20 bar. $\gamma = -0.4$ was used.

TABLE 6

Results of Power Law Estimate (in the Parameter Estimate the Apparent Reaction Order of CO Has Been Fixed to Unity)

	Pressure (bar)	E_a (kJ/mol)	α_{CO}	$\alpha_{\mathrm{H_2O}}$	$\alpha_{\mathrm{CO_2}}$	$\alpha_{\mathrm{H_2}}$
$Cu/ZnO/Al_2O_3$	5	86.5	1	1.4	−0.7	−0.9
$Cu/ZnO/Al_2O_3$	20	78.2	1	1.5	−0.7	−0.7
Cu/Al_2O_3	20	59.3	1	1.9	−1.4	−0.9

3.3. Results and Discussion

The agreement between the calculated exit mole fraction of CO from the microkinetic model and the experimental exit mole fraction of CO is shown in Fig. 1 for the $Cu/ZnO/Al_2O_3$ catalyst, in Fig. 2 for the Cu/Al_2O_3, and in Fig. 3 for the Cu/SiO_2 catalyst. In the microkinetic model the only free parameter is the Cu surface area of the catalyst. Generally there is reasonably good agreement between the calculated and the measured exit mole fraction of CO for all three catalyst systems.

A comparison of the estimated initial Cu surface area from the microkinetic model and the measured Cu surface area after reduction for the three catalysts is shown in Table 7. It should be noted that the Cu particles are found to sinter when they are exposed to the water–gas shift conditions (19). Thus the actual initial Cu surface area after exposure to the water–gas shift gas may be less than

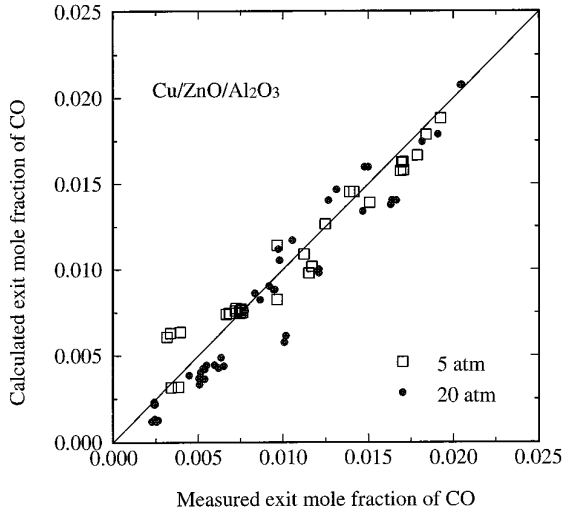

FIG. 1. Calculated (from the microkinetic model) and experimental exit mole fraction (in wet gas) of CO for experiments at 5 atm (squares) and 20 atm (circles) for $Cu/ZnO/Al_2O_3$.

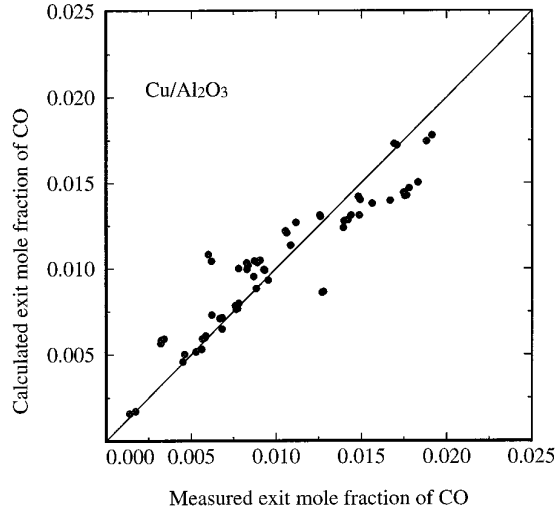

FIG. 2. Calculated (from the microkinetic model) and experimental exit mole fraction (in wet gas) of CO for experiments at 20 atm for Cu/Al_2O_3.

the area measured after reduction. From Table 7 it is seen that the estimated surface area agrees within a factor of two with the measured surface area. It is surprising that despite the severe constraints placed on the microkinetic model one can predict the rate of the shift reaction within a factor of two. Together with the kinetic analysis this result demonstrates that metallic copper is a useful starting point for modeling the water–gas shift reaction.

In the following we use the microkinetic model to analyze the reaction with respect to surface coverage of intermediates during reaction, the activation enthalpy, and

TABLE 7

A Comparison of the Measured Initial Cu Surface Area after Reduction Using the H_2-TPD Method and the Initial Cu Surface Area Determined from the Microkinetic Model

	Cu surface area	
Catalyst	By H_2-TPD (m^2/g cat)	By microkinetic model (m^2/g cat)
$Cu/ZnO/Al_2O_3$	10	10
Cu/Al_2O_3	15	8
Cu/SiO_2	5	4

reaction orders. This may elucidate the important intermediates during reaction and the origin of reaction orders and activation enthalpy.

Figure 4 shows a calculation of the surface coverage of intermediates as a function of pressure for a typical gas-phase composition and temperature. At low pressure hydrogen and hydroxide are the dominating intermediates whereas at high pressure hydrogen and adsorbed formate are the dominating intermediates. Formate is rather strongly bonded to the surface, and an increase in formate coverage decreases the coverage of free sites, which has an immediate consequence for the overall activation enthalpy (Fig. 5) and the reaction orders of the reaction (Fig. 6). Although formate may be synthesized from the gas phase through reaction between CO_2 and H_2, via reactions 5, 8 and 9, or from CO and H_2O through reactions 1, 2, 3, 6, 7 and 9, the former sequence is the more important. This

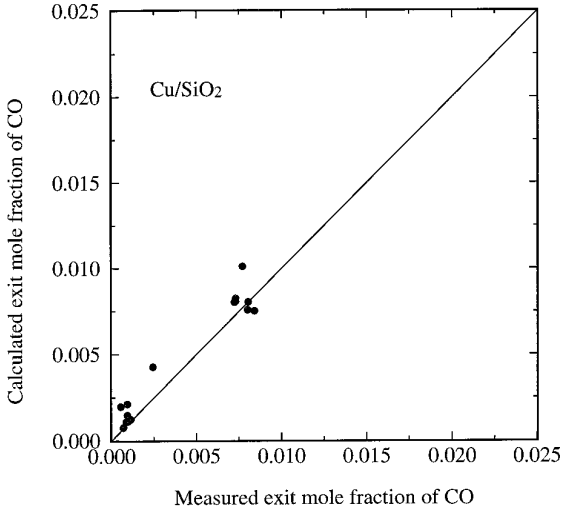

FIG. 3. Calculated (from the microkinetic model) and experimental exit mole fraction (in wet gas) of CO for experiments at 20 atm for Cu/SiO_2.

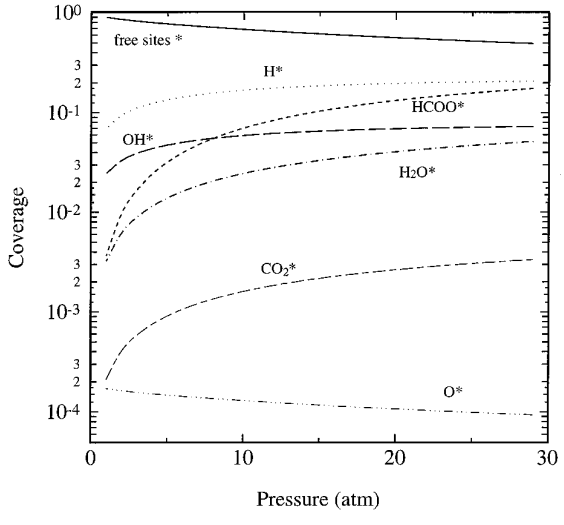

FIG. 4. The coverage of formate (---), hydrogen (···), hydroxide (————), water (–·–), carbon dioxide (—·—), oxygen (··–··), and free sites (—) as a function of total pressure for a catalyst operating at 220°C and 33% H_2O, 52% H_2, 13% CO_2, and 1% CO.

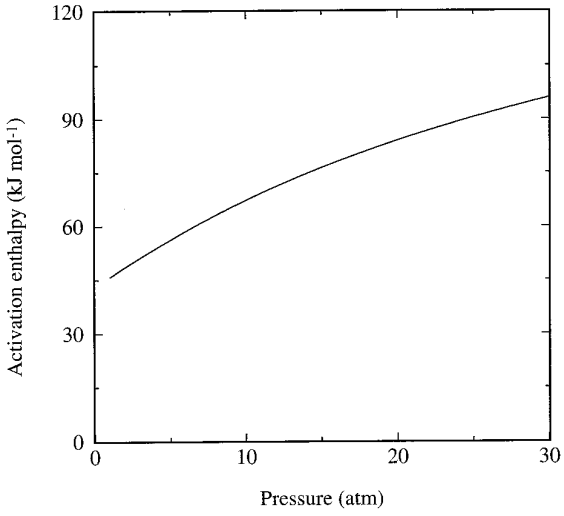

FIG. 5. The activation enthalpy as a function of total pressure for a catalyst operating at 220°C and 33% H_2O, 52% H_2, 13% CO_2, and 1% CO.

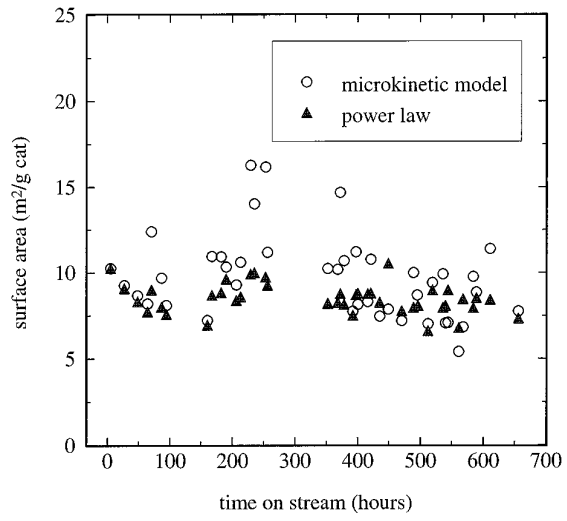

FIG. 7. Cu surface area necessary to reproduce each activity measurement. (○) Microkinetic model, (▲) power law model. Reaction data set 2 for $Cu/ZnO/Al_2O_3$.

means that an increase in the partial pressure of CO_2 and H_2 will increase the coverage of formate, which affects the reaction orders as shown in Table 4. This result is in good agreement with TPD measurements of an operating shift catalyst (at 5 atm) where formate was observed (30).

The reaction orders for CO and H_2O are close to unity, which reflect that, under the conditions considered here, reaction 7 (the oxidation of CO) is rate limiting. However, the rate of reaction 2 (the dissociation of H_2O) is not much faster than the rate of reaction 7.

The overall activation enthalpy as a function of pressure is shown in Fig. 5. Again the buildup of formate with increasing pressure is reflected as an increase of the overall activation enthalpy with pressure.

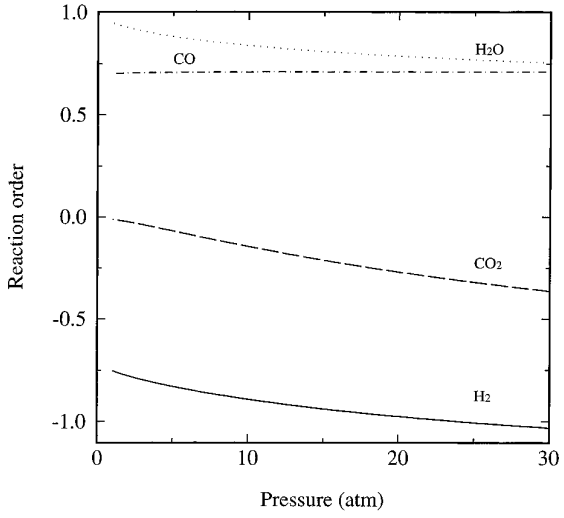

FIG. 6. The reaction orders for CO (–·–), H_2O (···), H_2 (———), and CO_2 (---) as a function of total pressure for a catalyst operating at 220°C and 33% H_2O, 52% H_2, 13% CO_2, and 1% CO.

As can be seen from Figs. 1–3, the microkinetic model does not give a perfect representation of the kinetic data. For this reason, we analyze in more detail the deviations between the microkinetic model and the reaction data and discuss the possible reasons for the deviations. First we express the ability of the microkinetic model to reproduce the kinetic data quantitatively. We note that the rate of the reaction is proportional with the surface area. An estimate of the surface area that gives perfect agreement of the model with the activity measurement can therefore be used as a quantitative measure of the ability of the model to describe the rate.

Figure 7 shows the estimated surface area for each activity measurement for reaction data for the $Cu/ZnO/Al_2O_3$ catalyst, Fig. 8 for reaction data for the Cu/Al_2O_3 catalyst, and Fig. 9 for reaction data for the Cu/SiO_2 catalyst. In Figs. 7 and 8 we also show the results from the power law estimate for reaction data for respectively the $Cu/ZnO/Al_2O_3$ catalyst and the Cu/Al_2O_3 catalyst. It is seen that the power law models give an excellent representation of the kinetic data for both catalysts. In comparison the microkinetic model shows larger scattering, which is not surprising considering the simplicity of the microkinetic model.

The ability of the microkinetic model in describing the reaction data over the $Cu/ZnO/Al_2O_3$ catalyst is summarized in Table 8. This table shows the relative change in surface area necessary for reproducing the kinetic measurement when the partial pressure of one component in the gas phase is changed from the highest to the lowest value in the data set. When evaluating these results, it is

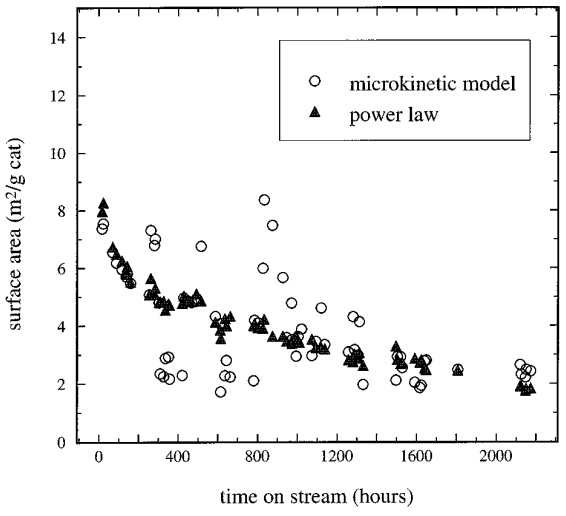

FIG. 8. Cu surface area necessary to reproduce each activity measurement. (○) Microkinetic model, (▲) power law model. Reaction data for Cu/Al_2O_3.

TABLE 8

The Ability of the Microkinetic Model to Describe the Reaction Data over the $Cu/ZnO/Al_2O_3$ Catalyst

Gas composition	180°C, 5 bar	211°C, 5 bar	180°C, 20 bar	214°C, 20 bar
$S/DG = 0.2$, CO_2 varied	0.99	1.38	0.64	1.08
$S/DG = 0.2$, H_2 varied	0.69	1.00	0.48	0.70
$S/DG = 0.5$, CO_2 varied	1.36	1.58	1.25	1.19
$S/DG = 0.5$, H_2 varied	0.68	0.87	0.51	0.76
S/DG varied	0.76	0.69	0.82	0.80

Note. The table shows the ratio between the estimated surface areas for two kinetic measurements where the reacting gas has respectively a low and a high concentration of one component in the gas phase. For constant temperature, total pressure and steam to dry gas ratio (S/DG) the partial pressure of CO_2 or the partial pressure of H_2 has been varied. Furthermore, at constant temperature and total pressure the steam to dry gas ratio has been varied for a dry gas with standard composition.

important to note that there is uncertainty on the experimental measured rate which is estimated to be approximately 10%. From Table 8 it is seen that the deviation in many cases is larger than the experimental uncertainty but all deviations are within a factor of two. We find that there is a tendency to underestimate the activity increase when decreasing the CO_2 partial pressure, suggesting that the reaction order for CO_2 should be more negative. We also note that there is a tendency to overestimate the activity increase when decreasing the partial pressure of H_2, suggesting that the reaction order for H_2 should be less negative. Finally, we find that there is a tendency for the microkinetic model to underestimate the activity increase when increasing the steam to dry gas ratio. This could reflect that the reaction order for water is too low. However, since in these experiments we vary all the partial pressures simultaneously (although the variation in the partial pressure of water is the largest) the discrepancy could also reflect that the reaction order for CO_2 should be more negative. A similar analysis of the reaction data for the Cu/Al_2O_3 catalyst shows that the deviations are within a factor of two.

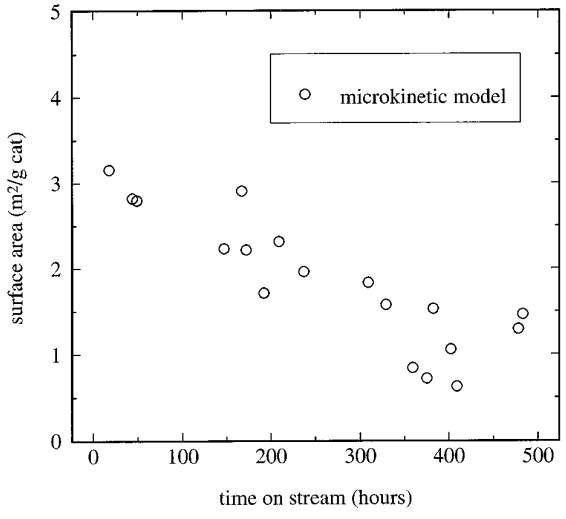

FIG. 9. Cu surface area necessary to reproduce each activity measurement. (○) Microkinetic model. Reaction data for Cu/SiO_2.

It is enlightening that the microkinetic model based on a mechanism where all the elementary steps have been observed experimentally and where all model parameters are determined from the kinetics and thermodynamics of the elementary steps can reproduce the observed kinetic variations within a factor of two. This suggests that the model describes many of the essential aspects of the water–gas shift reaction.

There may be several reasons for the observed deviations. One possibility could be that the microkinetic model based on a Langmuir–Hinshelwood kinetic description neglecting coverage dependent kinetic parameters is too simple. An improved description would then require a more advanced statistical mechanical treatment taking into account effects, such as adsorbate–adsorbate interactions.

Another possibility is that the mechanism deduced from model studies at low pressure on Cu single crystals is too simple and other intermediates or reaction paths are possible at high pressure. To investigate this possibility there is a need for high pressure studies *in situ.*

Finally, it is possible that reconstructions and morphology changes take place during synthesis. Recently, *in situ* EXAFS experiments showed that the particle morphology of the Cu particles supported on ZnO dynamically changes

depending on the gaseous environment (31). This dynamic morphology change of the Cu particles was observed to be support dependent since it was not observed for Cu supported on SiO_2. In the future it would seem interesting to study morphology changes of copper supported on Al_2O_3 and mixed ZnO/Al_2O_3. Using the *in situ* cell described in Ref. (32) it should furthermore be possible to perform simultaneously the kinetic and the *in situ* studies and such experiments should therefore be able to elucidate whether such morphology changes affect the kinetic measurements.

4. CONCLUSIONS

The water–gas shift reaction has been studied under industrial conditions over three different Cu-based catalysts. The kinetic data have been analyzed using a microkinetic model and a macroscopic power law model. The power law model gives a good fit of the kinetic data. The microkinetic analysis shows that it is possible to explain many of the basic trends of the water–gas shift reaction under industrial conditions using the surface redox mechanism deduced from Cu single-crystal studies including the synthesis and hydrogenation of formate and with the energetics of the elementary steps determined from Cu single-crystal studies. Furthermore, the deduced number of active sites agrees within a factor of two with the initial Cu surface area of the reduced catalysts determined separately. This suggests that a good starting point in interpreting the water–gas shift kinetics is to consider the catalysis as occurring solely on the metallic copper for Cu-based catalyst. The nature of the support may, however, have important secondary roles as evidenced in separate EXAFS experiments.

APPENDIX

In this appendix a selection of the reaction data for the $Cu/ZnO/Al_2O_3$ catalyst is tabulated. The full data set for all the three catalysts can be obtained from Haldor Topsøe A/S on request.

The following symbols are used:

Run-hr: time on gas.

Temp: temperature of reactor.

Pressure: total pressure.

SV: Normalized space velocity. The space velocity has been normalized so that the first measured activity has a space velocity of 1000 arbitrary units.

S/DG: Steam to dry gas ratio.

DG_{in}: inlet dry gas composition.

CO_{out}: Percentage CO in outlet dry gas.

Reaction Data Set 1

Catalyst: $Cu/ZnO/Al_2O_3$.
Inlet dry gas compositions:
A: 2.73% CO, 23.37% CO_2, 73.90% H_2.
B: 1.96% CO, 22.77% CO_2, 41.70% H_2, 33.57% He.
C: 2.41% CO, 11.30% CO_2, 73.00% H_2, 13.29% He.

Run-hr (hr)	Temp (°C)	Pressure (bar)	SV	*S*/DG	DG_{in}	CO_{out} (%)
21	181	20.9	978	0.47	A	1.86
29	198	21.2	988	0.46	A	1.39
46	215	21.2	1003	0.46	A	0.78
96	197	20.8	988	0.19	A	2.27
103	181	20.8	997	0.19	A	2.44
114	214	20.8	999	0.19	A	1.95
145	215	21.0	1007	0.46	A	0.77
166	180	20.9	1017	0.44	B	1.20
171	214	21.3	1036	0.44	B	0.35
189	214	20.9	1010	0.46	A	0.87
212	180	20.8	1020	0.20	B	1.76
215	214	21.0	1026	0.20	B	1.21
229	214	20.8	1010	0.47	A	0.91
327	180	20.6	992	0.47	C	1.43
330	215	20.8	992	0.47	C	0.36
337	215	21.1	953	0.50	A	0.76
354	180	20.7	994	0.19	C	2.16
360	214	21.0	1012	0.19	C	1.44
378	213	20.6	1011	0.45	A	0.92

Reaction Data Set 2

Catalyst: $Cu/ZnO/Al_2O_3$.
Inlet dry gas compositions:
D: 2.50% CO, 21.80% CO_2, 75.70% H_2.
E: 1.96% CO, 22.77% CO_2, 41.70% H_2, 33.57% He.
F: 2.41% CO, 11.30% CO_2, 73.00% H_2, 13.29% He.

Run-hr (hr)	Temp (°C)	Pressure (bar)	SV	*S*/DG	DG_{in}	CO_{out} (%)
70	184	20.6	1003	0.45	D	1.53
86	192	20.6	1006	0.46	D	1.34
94	210	20.7	1010	0.45	D	0.78
190	184	5.3	1000	0.46	D	1.82
206	193	5.2	997	0.46	D	1.64
213	211	5.3	1001	0.45	D	1.04
229	211	5.3	996	0.46	F	0.46
235	184	5.2	1000	0.46	F	1.41
253	211	5.1	1003	0.46	F	0.49
368	211	5.3	1004	0.45	D	1.08
392	184	5.2	1014	0.18	F	2.17
397	211	5.3	1009	0.18	F	1.64
421	212	5.3	1016	0.44	D	1.04
449	184	5.2	1010	0.19	D	2.29
470	211	5.2	1002	0.19	D	2.03
489	211	5.3	1007	0.45	D	1.10
512	184	5.4	1021	0.44	E	1.39
519	211	5.5	1029	0.44	E	0.49
536	211	5.2	1002	0.46	D	1.09
561	183	5.5	1029	0.18	E	1.78
568	210	5.5	1041	0.19	E	1.37
584	211	5.2	1008	0.46	D	1.11
656	211	20.2	1004	0.47	D	0.74

ACKNOWLEDGMENTS

We appreciate many discussions with S. L. Andersen, J. B. Hansen, J. H. B. Hansen, P. E. Højlund Nielsen, H. Topsøe, and E. Törnqvist. Financial support has been provided by the Danish Research Councils through the Center for Surface Reactivity.

REFERENCES

1. Bohlbro, H., and Jørgensen, M. H., *Chem. Eng. World* **5,** 46 (1970).
2. Newsome, D. S., *Catal. Rev. Sci. Eng.* **21,** 275 (1980).
3. Twigg, M. V., Ed., ''Catalyst Handbook,'' 2nd ed. Wolfe, England, 1989.
4. Carstensen, J. H., Hansen, J. B., and Pedersen, P. S., *Ammonia Plant Saf.* **31,** 113 (1991).
5. van Herwijnen, T., and de Jong, W. A., *J. Catal.* **63,** 83 (1980).
6. Grenoble, D. C., Estadt, M. M., and Ollis, D. F., *J. Catal.* **67,** 90 (1981).
7. Fiolitakis, E., and Hofmann, H., *J. Catal.* **80,** 328 (1983).
8. Hadden, R. A., Vandervell, H. D., Waugh, K. C., and Webb, G., *in* ''Proceedings, 9th International Congress on Catalysis, Calgary, 1988'' (M. J. Phillips and M. Ternan, Eds.), Vol. 4, p. 1835. Chem. Institute of Canada, Ottawa, 1988.
9. Salmi, T., and Hakkarainen, R., *Appl. Catal.* **49,** 285 (1989).
10. Nakamura, J., Campbell, J. M., and Campbell, C. T., *J. Chem. Soc. Faraday Trans.* **86,** 2725 (1990).
11. Dumesic, J. A., Rudd, D. F., Aparicio, L. M., Rokoske, J. E., and Treviño, A. A., ''The Microkinetics of Heterogeneous Catalysis.'' Am. Chem. Soc., Washington, DC, 1993.
12. Boudart, M., and Djéga-Mariadassou, G., ''Kinetics of Heterogeneous Catalytic Reactions.'' Princeton Univ. Press, Princeton, NJ, 1984.
13. Stoltze, P., *Phys. Scr.* **36,** 824 (1987).
14. Dumesic, J. A., Topsøe, N.-Y., Slabiak, T., Morsing, P., Clausen, B. S., Törnqvist, E., and Topsøe, H., *in* ''Proceedings, 10th International Congress on Catalysis, (L. Guczi, F. Solymosi, and P. Tétényi, Eds.), p. 1325. Akadémiai Kiadó, Budapest, 1993.
15. Rostrup-Nielsen, J., *in* ''Elementary Reaction Steps in Heterogeneous Catalysis,'' pp. 441–460. Kluwer Academic, The Netherlands, 1993.
16. Ovesen, C. V., Stoltze, P., Nørskov, J. K., and Campbell, C. T., *J. Catal.* **134,** 445 (1992).
17. Rasmussen, B. S., Højlund Nielsen, P. E., Villadsen, J., and Hansen, J. B., *in* ''Preparation of Catalysts'' (B. Delmon, P. Grange, P. A. Jacobs, and G. Poncelet), Vol. IV, p. 785. Elsevier, Amsterdam, 1987.
18. Wielers, A. F. H., Mesters, C. M. A. M., Koebrugge, G. W., van der Grift, C. J. G., and Geus, J. W., *in* ''Preparation of Catalysts'' (B. Delmon, P. Grange, P. A. Jacobs, and G. Poncelet, Eds.), Vol. IV, p. 401. Elsevier, Amsterdam, 1987.
19. Muhler, M., Nielsen, L. P., Törnqvist, E., Clausen, B. S., and Topsøe, H., *Catal. Lett.* **14,** 241 (1992).
20. Askgaard, T. S., Nørskov, J. K., Ovesen, C. V., and Stoltze, P., *J. Catal.,* **156,** 229 (1995).
21. Taylor, P. A., Rasmussen, P. B., Ovesen, C. V., Stoltze, P., and Chorkendorff, I., *Surf. Sci.* **261,** L191 (1992).
22. Millar, G. J., Rochester, C. H., and Waugh, K. C., *Catal. Lett.* **14,** 289 (1992).
23. Nakamura, J., Rodriguez, J. A., and Campbell, C. T., *J. Phys. Condens. Matter* **1,** SB149 (1989).
24. Taylor, P. A., Rasmussen, P. B., and Chorkendorff, I., *J. Vac. Sci. Technol. A* **10,** 2570 (1992).
25. Bowker, M., Hadden, R. A., Houghton, H., Hyland, J. N., and Waugh, K. C., *J. Catal.* **109,** 263 (1988).
26. Chorkendorff, I., Taylor, P. A., and Rasmussen, P. B., *J. Vac. Sci. Technol. A* **10,** 2277 (1992).
27. Rasmussen, P. B., Holmblad, P. M., Askgaard, T., Ovesen, C. V., Stoltze, P., Nørskov, J. K., and Chorkendorff, I., *Catal. Lett.* **26,** 373 (1994).
28. Ruckenstein, E., *in* ''Metal-Support Interactions in Catalysis, Sintering, and Redispersion'' (S. A. Stevenson, J. A. Dumesic, R. T. K. Baker, and E. Ruckenstein, Eds.) p. 165. Van Nostrand–Reinhold, New York, 1987.
29. Bohlbro, H., ''An Investigation on the Kinetics of the Conversion of Carbon Monoxide with Water Vapour over Iron Oxide Based Catalysts.'' Gjellerup, Copenhagen, 1966.
30. Muhler, M., and Törnqvist, E., in preparation.
31. Clausen, B. S., Gråbæk, L., Ovesen, C. V., Schiøtz, J., Jacobsen, K. W., and Nørskov, J. K., *Topics Catal.* **1,** 367 (1994).
32. Clausen, B. S., Steffensen, G., Fabius, B., Villadsen, J., Feidenhans'l, R., and Topsøe, H., *J. Catal.* **132,** 524 (1991).